Phased Subarray Processing for Underwater 3D Acoustic Imaging

Jeremy A. Johnson[1,2], Mustafa Karaman[1], B. T. Khuri-Yakub[1]

[1]Ginzton Laboratory, Stanford University, Stanford, CA 94305-4088
[2]Image Guidance Laboratory, Stanford University, Stanford, CA 94305

Abstract—**3D sonar imaging using a fully-populated rectangular 2D array has many promising applications for underwater imaging. A primary limitation of such systems is the large number of parallel front-end hardware channels needed to process the signals in transmit and receive when using conventional full phased array imaging. A subaperture beam acquisition and image formation process is presented that significantly reduces the number of front-end hardware channels while achieving image quality approaching that of full phased array imaging. Rather than transmitting and receiving on all $N \times N$ transducer elements to form each beam, an $M \times M$ subset of elements—called a subarray—is used for each firing. The limited number of front-end processing channels are used to acquire data from each subarray. Switching hardware allows the subarray to be multiplexed across the full array. Due to the Nyquist sampling criteria in beamspace, the number of beams acquired by each subarray can be significantly reduced compared to the number required for the full array. The phased subarray processing includes beam upsampling, lateral interpolation with a subarray-dependent filter, and coherent weighting and summation of all subarray images to form a high resolution image. The phased array method achieves an image quality nearing that of full phased array imaging with significantly fewer processing channels, slightly reduced SNR, and roughly three times the number of firings for reasonable configurations.**

I. Introduction

High-performance 3D sonar imaging could be applied to a number of underwater applications. Unmanned undersea vehicles (UUVs) could use 3D imaging for improved obstacle avoidance, mine detection and reconnaissance, and navigation. Divers could use a handheld 3D sonar imaging system for navigation in low visibility conditions, such as in shallow waters, rivers, or ports. Forward-looking 2D acoustic transducer arrays are a promising technology for 3D underwater imaging.

One of the primary constraints of 2D array imaging systems is the overwhelming number of front-end hardware channels that are necessary to process the transmitted and received signals in real time [1]. Another difficulty has been addressing all transducer channels individually. One active research topic aiming to address these problems by using a reduced number of transducers is the design of sparse arrays [2-4]; current results show that these often suffer from high side lobes. Recent work has been done to electrically address a fully-populated 2D rectangular array [5]. The method presented here uses such a fully-populated transducer array, but still uses a reduced number of front-end hardware channels.

In this paper we present a method of reconstructing 3D acoustic images by acquiring signals from a small subset of array elements at any given time. By reducing the number of parallel transmit and receive channels used during a single beam formation, the number of front-end processing channels can be significantly reduced. The purpose of this new imaging method is to sufficiently reduce the front-end complexity—and thus size, cost, and power consumption—such that real-time 3D sonar imaging can become a reality.

In conventional full phased array (FPA) imaging, all transducer elements simultaneously transmit properly-delayed pulses to steer and focus an acoustic beam toward a desired location. Likewise, all transducer elements simultaneously receive the reflected acoustic signal to form a dynamically-focused receive beam. Each transmit/receive "firing event" is repeated, each time steering the beam to a new location. The beams are then combined to form the resultant image [6, 7].

The proposed phased subarray (PSA) imaging method described in this paper is based on other studies using synthetic subaperture imaging for 2D imaging [8, 9]. When applied to 3D imaging, a fully-populated rectangular array is subdivided into a number of overlapping subarrays, each composed of a group of adjacent transducer elements. For each firing event, only a single subarray is used for transmit and receive beamforming. Due to the reduced transmit and receive aperture size, a smaller number of beams need be acquired as determined by the Nyquist sampling criteria without any loss of information. The unacquired beams can be reconstructed by upsampling and interpolation using a subarray-dependent set of filters. Each subarray acquires a different range of spatial frequency components. The spatial frequency range of the combined set of subarrays equals that of the full array. Therefore, by combining the reconstructed subarray images, the response of PSA imaging is equivalent to that of FPA imaging.

The paper is organized as follows. Phased subarray acquisition is described in more detail in Section II.A. Section II.B discusses the 3D frequency response of 2D rectangular arrays. The frequency response resulting from each stage of PSA image formation is presented in Section II.C. The performance of the method is compared to FPA imaging in Section III, and closing remarks are made in Section IV.

II. Methods

A. Subarray Beam Acquisition and Processing

An $N \times N$ fully-populated two-dimensional transducer array with element pitch d is subdivided into $K \times K$ square subarrays, each with $M \times M$ elements. The subarrays overlap by half the subarray width ($M/2$) in both directions, and thus the following equation relates N, K, and M:

0-7803-7534-3/$10.00©2002 IEEE

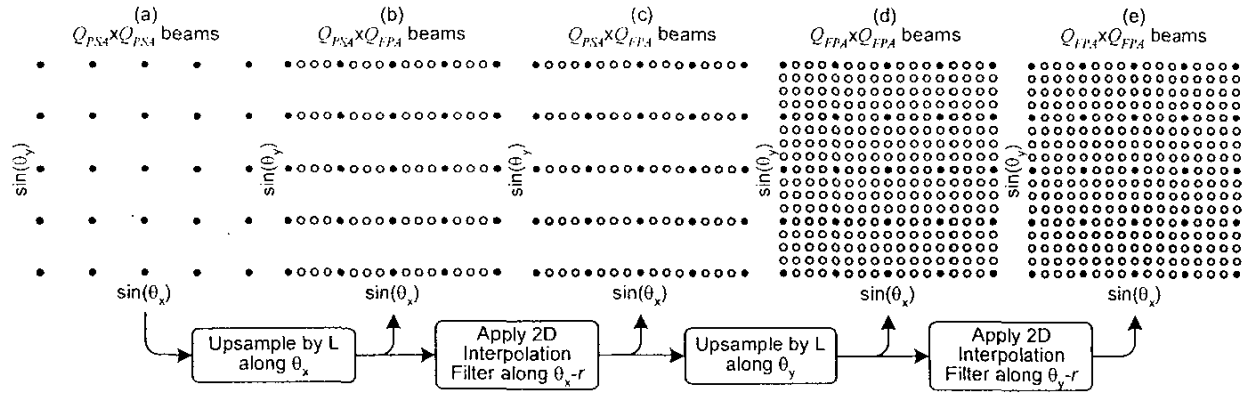

Figure 1. Beam processing for PSA image reconstruction. Each point represents a single beam that extends radially from the center of the array.

$$M(K+1)=2N \tag{2.1}$$

The array lies centered on the x-y plane, and faces the positive z axis.

Each subarray transmits and receives from all of its elements to form acoustic beams that sweep out a sector of size $\Theta\times\Theta$. The beams all begin at the array center and are directed outward with steering angles θ_x and θ_y measured from the array normal toward the x- and y-axes, respectively. The steering angles are evenly spaced in $\sin\theta_x$ and $\sin\theta_y$. The received signals are sampled in time such that beams can be reconstructed to a depth of R. The transmit and receive beamforming delays for each element are identical to those that would be used for FPA imaging. The received acoustic signals from all subarray elements are appropriately delayed and summed to form each beam. Prior to additional processing, a Hilbert transform filter is applied to form an analytic signal with only positive frequency components.

The Nyquist sampling criteria requires that the following number of beams be acquired in each dimension:

$$Q_{FPA} > \frac{4Nd}{\lambda_{\min}}\sin\left(\frac{\Theta}{2}\right), \tag{2.2}$$

where $\lambda_{\min}$ is the acoustic wavelength corresponding to the maximum frequency component, and Q_{FPA} is the number of beams acquired for FPA imaging using an array with N elements in the beam sweep direction. For a single subarray using PSA imaging, the number of beams required per dimension is reduced to

$$Q_{PSA} > \frac{4Md}{\lambda_{\min}}\sin\left(\frac{\Theta}{2}\right). \tag{2.3}$$

Each subarray first acquires $Q_{PSA}\times Q_{PSA}$ beams, as illustrated in Fig. 1(a). The object is to upsample the subarray images formed by these beams and reconstruct a fully-sampled 3D image with $Q_{FPA}\times Q_{FPA}$ beams using a specially-designed filter.

The most straightforward method of reconstruction would be upsampling the subarray images in both the θ_x and θ_y dimensions and convolving with a 3D FIR filter. The 3D filter is separable in θ_x and θ_y such that the reconstruction filtering can be performed by applying two different 2D filters along the two dimensions sequentially. This process greatly reduces the number of computations required to apply the filter.

Each subarray image is upsampled along θ_x by a factor of L by inserting $L-1$ zero-valued beams between the acquired beams (Fig. 1(b)). The upsampling rate is determined by the ratio of the number of beams required for the full array and each subarray:

$$L=\left\lceil\frac{Q_{FPA}}{Q_{PSA}}\right\rceil=\left\lceil\frac{N}{M}\right\rceil, \tag{2.4}$$

where $\lceil x\rceil$ is the ceiling function. The subarray-dependent 2D FIR filter $h_k[q_x,r]$ is applied to each θ_x-r plane in order to interpolate the missing beams (Fig. 1(c)). Ideally, this reconstructed image would be equal to an image formed by directly acquiring $Q_{FPA}\times Q_{PSA}$ beams.

The same upsampling/interpolation process is then applied in the θ_y direction (Fig. 1(d-e)). A second 2D FIR filter $h_k[q_y,r]$ is applied in the θ_y direction to reconstruct these missing beams. All subarray images are now equivalent to what they would have been had each directly acquired the full set of $Q_{FPA}\times Q_{FPA}$ beams. Given a sufficiently fast digital signal processor (DSP), the beam upsampling and interpolation of a single subarray image can be performed in less time than the pulse-echo propagation time of $Q_{PSA}\times Q_{PSA}$ beams. As a result, the time required to form complete $Q_{FPA}\times Q_{FPA}$-beam images is significantly reduced, in turn increasing the frame rate.

The final step in forming the 3D image is to weight and sum all $K\times K$ subarray images. The weights are given by

$$w[k_x,k_y]=\left(K-\left|k_x-\frac{K+1}{2}\right|\right)\left(K-\left|k_y-\frac{K+1}{2}\right|\right), \tag{2.5}$$

where k_x and k_y are the subarray indices in the x and y directions, respectively, and range from 0 to $K-1$. This choice of weights is justified in Section II.C.

The resultant image is equivalent to that formed by acquiring $Q_{FPA} \times Q_{FPA}$ beams from the full $N \times N$-element array using FPA image formation. The advantage of using PSA image formation is that fewer front-end processing channels are required—only $M \times M$ instead of $N \times N$—and with a tolerable decrease in frame rate.

B. 3D Frequency Domain Array Response

The equivalence of PSA imaging to FPA imaging and the PSA filter design is more clearly illustrated in the 3D spatial frequency domain. We first consider the 2D lateral frequency response. The far-field 2D two-way lateral point spread function (PSF) is directly related to the transmit and receive aperture functions via the Fourier transform:

$$U\left[q_x, q_y\right] = \Im_{2D}\left\{\tilde{a}_T\left[n_x, n_y\right]\right\} \cdot \Im_{2D}\left\{\tilde{a}_R\left[n_x, n_y\right]\right\}, \quad (2.6)$$

where $\tilde{a}_T[\,]$ and $\tilde{a}_R[\,]$ are the 2D aperture functions. Compared to the array-sampled discrete aperture function, $a[\,]$, with a fixed sampling period d, the aperture function $\tilde{a}[\,]$ samples the aperture with a frequency-dependent period $\lambda/2$. This difference will have the effect of scaling the width of all derivative functions by $2d/\lambda$.

Consequently, the lateral frequency domain response—or *coarray* [10, 11]—is equal to the convolution of the aperture functions:

$$u\left[m_x, m_y\right] = \Im_{2D}\left\{U\left[q_x, q_y\right]\right\} \quad (2.7)$$

$$u\left[m_x, m_y\right] = \tilde{a}_T\left[n_x, n_y\right] \otimes\otimes \tilde{a}_R\left[n_x, n_y\right] \quad (2.8)$$

The coarray corresponding to the full $N \times N$ array is therefore equal the convolution of two squares, resulting in a pyramid-like function with a square base of width $2(2N-1)d/\lambda$. Similarly, the center subarray will have a *cosubarray* equal to a pyramid with base width $2(2M-1)d/\lambda$. Since the other subarrays are shifted in either direction by multiples of $M/2$, their cosubarrays are likewise shifted by multiples of $2Md/\lambda$, or half the width of the cosubarray. All cosubarrays overlap by half their width in both directions; in this arrangement, the full coarray is a linear combination of all cosubarrays. In other words, simply weighting and summing the subarray response results in the full array response. So far, the discussion has been limited to a single frequency.

In practice, the transmit pulse is a bandlimited signal with center frequency f_0 and ranging from $f_{\min}$ to $f_{\max}$. The wavelength varies with frequency,

$$\lambda = c/f\,, \quad (2.9)$$

and thus the 2D coarray at each frequency will be scaled and shifted linearly with increasing frequency. In addition, the coarrays at each frequency will be weighted by the relative contribution of the corresponding frequency of the excitation pulse. Let $U[r]$ be the axial impulse response of the system corresponding to the excitation pulse with sampling frequency f_s. The axial frequency response is then given by

$$u\left[m_r\right] = \Im\left\{U\left[r\right]\right\} \quad (2.10)$$

$U[r]$ is an analytic signal, and thus $u[m_r]$ has only positive frequency components. The overall 3D frequency response of a single transmission from one aperture to another is

$$u\left[m_x, m_y, m_r\right] = \left(\tilde{a}_T\left[n_x, n_y\right] \otimes\otimes \tilde{a}_R\left[n_x, n_y\right]\right) \cdot u\left[m_r\right]. \quad (2.11)$$

Recalling that the width of the modified aperture functions increases linearly with frequency, the expression in parentheses represents a 3D structure with a square lateral cross-section boundary (examples are shown in the left column of Fig. 2). Due to the linearly increasing width, the bounds of the structure define a square pyramid whose top is positioned at the origin and whose base extends toward the axial frequency axis, m_r. A bandlimited axial frequency response causes the top and the base of the pyramidal boundary to be clipped, reducing the bounds to a square pyramidal frustum. Figure 2(e) shows the cross sections of the 3D response for a full phased array system. For a subarray located at the center of the array, this frustum is aligned with the radial frequency axis. Shifting the subarray off axis has the effect of slanting the frustum away from the m_r axis. Figure 2(d) illustrates the effect of shifting the subarray towards the positive y axis, resulting in a slant of the frustum towards the positive m_y axis. Figures. It is important to observe that because the subarrays overlap by half their width, the corresponding frustums in 3D frequency space will also overlap by half their lateral width; as a result, the frustum corresponding to the full-array (FPA) response is a linear combination of the subarray responses.

C. 3D Frequency Domain PSA Processing

The frustum-bounded frequency-domain responses discussed thus far represent the subarray response when acquiring a full set of Q_{FPA} beams in each angular dimension. Sampling a reduced set of Q_{PSA} beams results in lateral expansion and circular wrapping of the response in the frequency domain. As a result, the lateral bounds of the frustum nearly extend to fill all of the lateral frequency space. Figure 2 shows three orthogonal cross sections through the center of 3D frequency space for each stage of PSA processing. The example shown gives the response of a single subarray located at the center of the full array in the x axis and at the edge of the array in the y axis ($k_x = 3$, $k_y = 6$). The response of the system when acquiring only $Q_{PSA} \times Q_{PSA}$ beams with this subarray is shown in Fig. 2(a). Since the subarray is not centered along the y axis, the frustum is slanted in the m_r-m_y plane. Properly choosing the beamsampling rate prevented the boundary of response from overlapping onto itself.

Lateral upsampling by a factor of L along a single spatial dimension, q_x, results in L periodic replicates of the frustum to be formed in frequency space along the dimension m_x, as shown in Fig. 2(b). The frustum response whose vertex is located at the origin is the desired response; all others are unwanted aliases. The purpose of the frequency-domain reconstruction filter, $H_k[m_x, m_r]$, is to eliminate the aliases. The frequency-domain response of the filter is therefore a rectangle centered over the desired frustum as indicated in Fig. 2(b). This process is repeated for all subarray images. As shown in Fig. 2(c), the aliases have been eliminated.

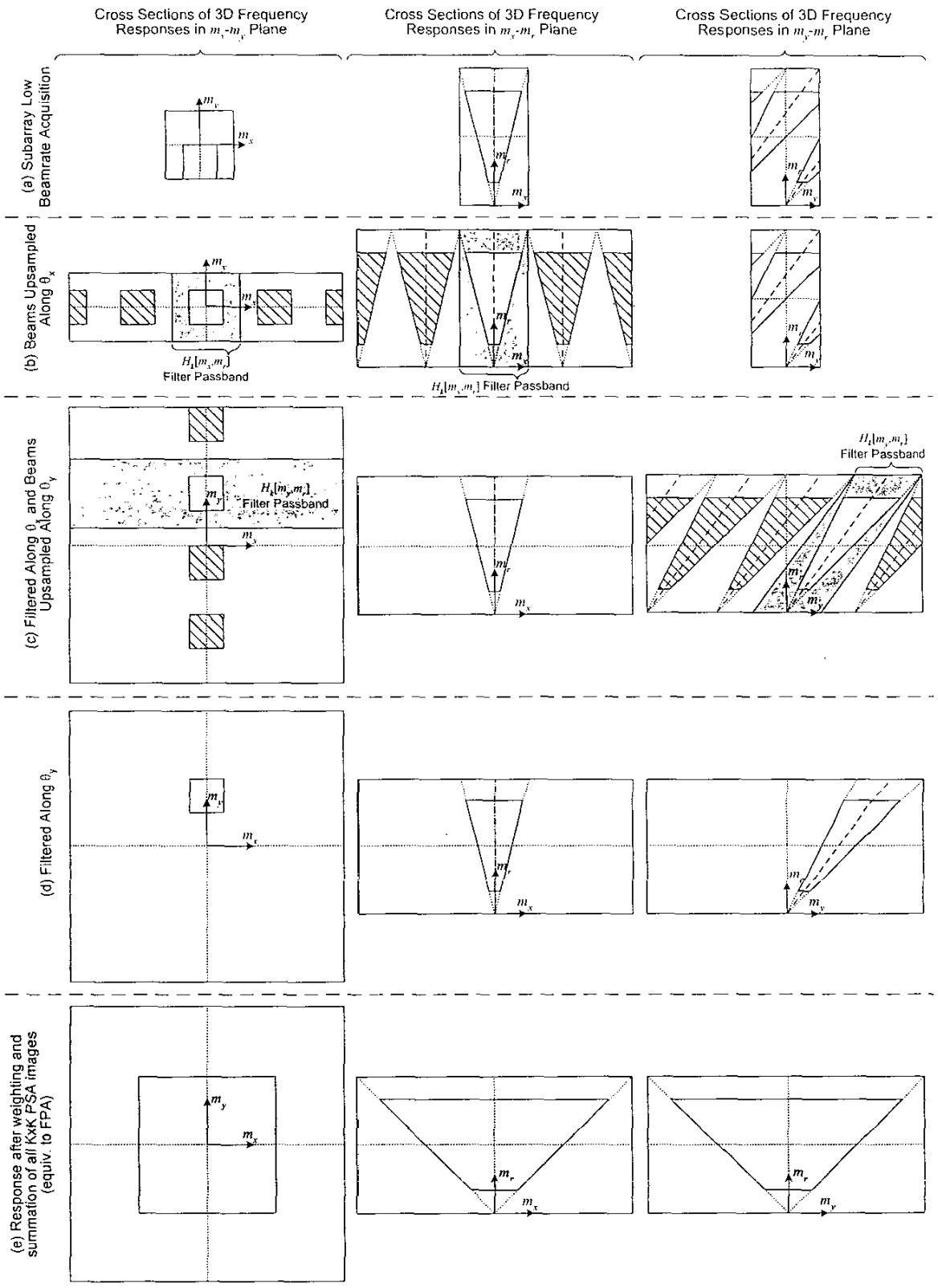

Figure 2. 3D frequency response at each stage of PSA processing. The light shaded regions represent the boundaries of the nonzero response region.

The process is repeated for the other lateral dimension, q_r. Again, L periodic replicates are formed in the frequency domain, this time along the m_r axis, as shown in Fig. 2(c). The reconstruction filter, $H_k[m_r,m_r]$, is applied to eliminate the $L-1$ aliases.

After upsampling and reconstruction filtering in both lateral directions, the combined frequency response for each subarray is equivalent to the response of a subarray that had directly acquired $Q_{FPA}\times Q_{FPA}$ beams directly. The frequency-domain response of the example subarray is shown in Fig. 2(d). That responses of all $K\times K$ subarrays can be linearly combined to form the FPA-equivalent response is made clear when considering a single lateral cross section through the 3D frequency-domain response. As discussed in the previous subsection, the bounds of the lateral response define a square, and the magnitude is pyramidal with a square base. Because the subarrays are spaced apart by half the subarray size, the square pyramids in the frequency domain corresponding to adjacent subarrays also overlap by half the width of the pyramid's base; this is true in both dimensions. As a result, the magnitude of the frequency domain at any point is found via bilinear interpolation of the four nearest pyramidal peaks. To achieve an FPA-equivalent frequency response—yet another square pyramid whose base is equal to the composite of bases of the subarray pyramids—the subarray responses must be weighted such that the magnitude of their corresponding pyramids define the surface of the full FPA pyramid. The proper subarray weights that achieve the full array response are given in (2.5).

Regardless of the frequency at which the cross section is observed, the principles of the 2D lateral subarray response still apply. Consequently, the linear combination of the subarray frustums using the specified weights will result in the full array response frustum. In other words, the combined PSA system frequency domain response is equivalent to that of an FPA imaging system.

III. Results

The proposed phased subarray 3D imaging method has been shown to have a theoretical response equivalent to that of full phased array imaging. The PSA imaging method achieves this result while significantly reducing the front-end hardware complexity. The required number of front-end hardware channels is reduced from N^2 for an FPA system to M^2.

The total number of firings required for each imaging method is equal to the total number of beams acquired:

$$B_{FPA}=Q_{FPA}^2=\left(\frac{4Nd}{\lambda_{\min}}\sin\left(\frac{\Theta}{2}\right)\right)^2 \tag{3.1}$$

$$B_{PSA}=K^2\cdot Q_{PSA}^2=\left(K\frac{4Md}{\lambda_{\min}}\sin\left(\frac{\Theta}{2}\right)\right)^2 \tag{3.2}$$

Although the subarray beam-sampling rate is significantly less than the rate required for the full array, the total number of subarray beams acquired is still higher than the number of full array beams. This increase can be expressed as

$$\frac{B_{PSA}}{B_{FPA}}=\left(\frac{KM}{N}\right)^2=\left(\frac{\left(\frac{2N}{M}-1\right)M}{N}\right)^2=\left(2-\frac{M}{N}\right)^2. \tag{3.3}$$

The number of PSA firings is therefore always less than 4 times the number of FPA firings; for a reasonable configuration with $M=N/4$, the increase is approximately 3 times.

For a general acoustic imaging system, the frame rate is limited by the number beams acquired and the time required for the acoustic signals to travel to the maximum imaging depth, R, and back:

$$F=\frac{c}{B\cdot 2R}, \tag{3.4}$$

where c is the sound velocity in the medium. As an example, consider a system employing a 32×32-element array subdivided into 7×7 subarrays each with 8×8 elements. Furthermore, the elements are spaced at $d=\lambda_{min}/2$; the imaging sector angle is 60°×60°; the velocity of sound is 1480 m/s; and the imaging depth is 1 m. Such a system would require 1,600 beams (40×40), resulting in one frame every two seconds.

Signal-to-noise (SNR) performance of an array imaging system is dependent upon the number of active transmit and receive channels. Assuming that the noise is additive and statistically independent on the receive channels, the SNR of an FPA system is given by

$$SNR_{FPA}=20\log_{10}\left[N^3\right]+SNR_0 \text{ (dB)}, \tag{3.5}$$

where SNR_0 is the pulse-echo SNR of a single channel, assuming that the SNR of the array channels are identical. For a 32×32-element full phased array system, the SNR is 90.3 dB above SNR_0. For the proposed PSA system, the relative SNR is given by

$$SNR_{PSA}=20\log_{10}\left[(2N-M)M^2\right]+SNR_0 \text{ (dB)} \tag{3.6}$$

For the previous PSA example with a 32×32-element array, the relative SNR is 88.0 dB above SNR_0. Therefore, PSA imaging has an SNR 2.3 dB below the equivalent FPA system.

Numerical simulations were performed to evaluate the point spread function. The array parameters were similar to those given in the example ($N=32$, $M=8$, $K=7$). The element spacing was $d=\lambda_0/2$, where λ_0 is the wavelength corresponding to the center frequency. The excitation pulse used was a modulated Gaussian with 50% bandwidth. A perfect point reflector was positioned directly in front of the array at a distance of $60.9\,\lambda_0$. The fixed transmit focal point was fixed at the position of the point reflector, and dynamic focusing was used on receive. Both FPA and PSA methods were simulated using the same array for comparison.

For FPA imaging, 129×129 beams ($Q_{FPA}\times Q_{FPA}$) were formed directly. For the PSA imaging simulations, only 33×33 beams ($Q_{PSA}\times Q_{PSA}$) were formed. These were upsampled by 4 (L) in each lateral dimension prior to filtering such

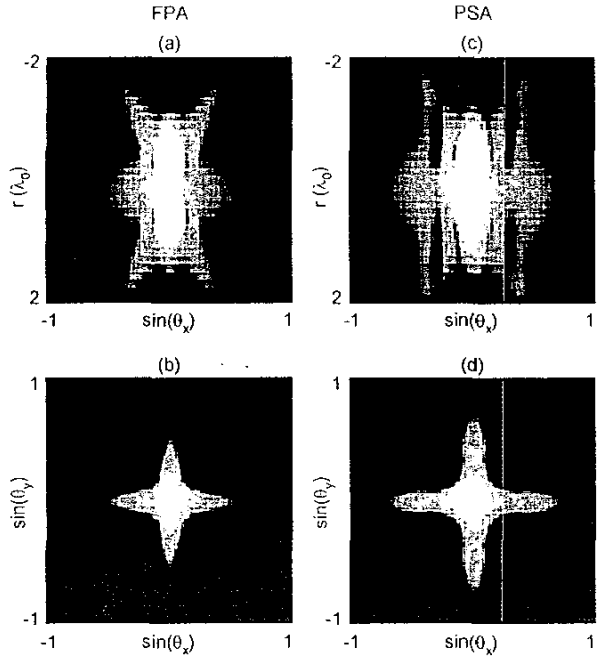

Figure 3. Cross sections of the 3D point spread function for FPA and PSA imaging methods. Images displayed with 50 dB of logarithmic compression.

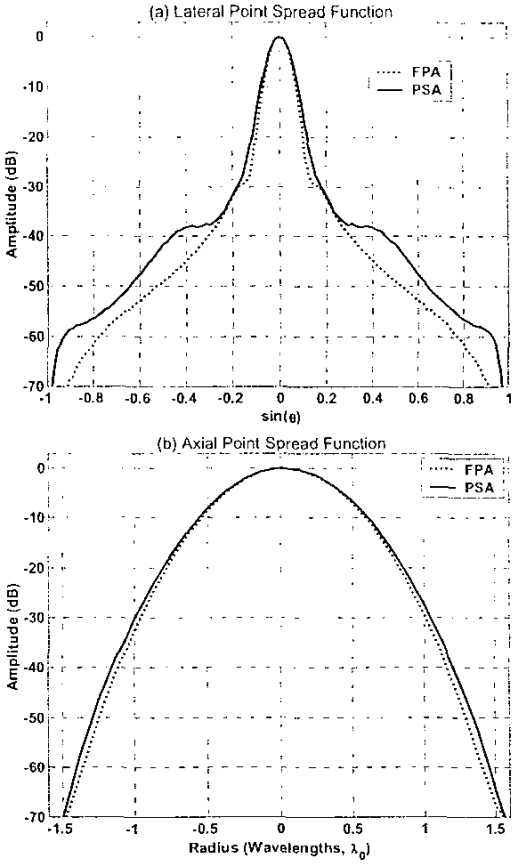

Figure 4. Lateral and axial point spread functions for FPA and PSA imaging.

that the final number of beams was the same as for FPA. The interpolation filters for each subarray were first calculated using the ideal filters as shown in Fig. 2. The inverse discrete Fourier transform was used to determine the spatial domain filters, which were subsequently truncated to 31 and 15 taps in the lateral and axial dimensions, respectively. A hamming window was also applied in both dimensions. Figure 3 shows cross sections through the raw beams centered at the location of the point reflector. The magnitude of the PSF has been plotted along the axial and lateral dimensions in Fig. 4. The axial response for the two methods is nearly identical, with 3-dB resolutions of 0.61 λ_0 and 0.63 λ_0 for FPA and PSA, respectively. The lateral PSFs are also nearly identical within the center 36° sector, with 3-dB resolutions of 2.22° and 2.48° for FPA and PSA, respectively. Beyond this range, however, this example of PSA suffers from wide side lobes.

IV. Discussion and Conclusion

We have presented a phased array imaging method for 3D imaging that greatly reduces the front-end hardware while achieving near-FPA resolutions. The SNR is slightly reduced, and the frame rate is reduced by a factor of 3 for reasonable configurations. The simulations show that the PSA method suffers from high outer lobes in the lateral response. These may be due to the small number of elements used, as these are not present in 1D array simulations with 128 elements using similar techniques [12].

The theory and examples provided in this paper all assumed a square 2D array with the same number of elements in both directions. Although this simplified discussions here, the principles equally apply to non-square rectangular arrays.

V. References

[1] M. E. Schafer and P. A. Lewin, "The influence of front-end hardware on digital ultrasonic imaging," *IEEE Transactions on Sonics and Ultrasonics*, pp. 295-306, 1984.

[2] P. Gori, G. Cincotti, and M. Pappalardo, "Dense and sparse 2-D array radiation patterns in lossy media," *IEEE Transactions on Ultrasonics, Ferroelectrics and Frequency Control*, vol. 47, pp. 940-8, 2000.

[3] A. Austeng and S. Holm, "Sparse arrays for real-time 3D imaging, simulated and experimental results," presented at 2000 IEEE Ultrasonics Symposium, San Juan, Puerto Rico, 2000.

[4] G. R. Lockwood, J. R. Talman, and S. S. Brunke, "Real-time 3-D ultrasound imaging using sparse synthetic aperture beamforming," *IEEE Transactions On*

Ultrasonics Ferroelectrics And Frequency Control, pp. 980-988, 1998.

[5] C. H. Cheng, E. M. Chow, X. Jin, S. Ergun, and B. T. Khuri Yakub, "An efficient electrical addressing method using through-wafer vias for two-dimensional ultrasonic arrays," *Proceedings of the IEEE Ultrasonics Symposium*, vol. 2, pp. 1179-1182, 2000.

[6] B. D. Steinberg, *Principles of Aperture and Array System Design : Including Random and Adaptive Arrays*. New York: Wiley, 1976.

[7] T. A. Shoup and J. Hart, "Ultrasonic imaging systems," presented at IEEE 1988 Ultrasonics Symposium, Chicago, IL, USA, 1988.

[8] M. Karaman, "Ultrasonic array imaging based on spatial interpolation," presented at 3rd IEEE International Conference on Image Processing, Lausanne, Switzerland, 1996.

[9] M. Karaman and O. D. M, "Subaperture processing for ultrasonic imaging," *IEEE Transactions On Ultrasonics Ferroelectrics And Frequency Control*, pp. 126-135, 1998.

[10] R. T. Hoctor and S. A. Kassam, "The unifying role of the coarray in aperture synthesis for coherent and incoherent imaging," *Proceedings of the IEEE*, vol. 78, pp. 735-52, 1990.

[11] R. J. Kozick and S. A. Kassam, "Synthetic aperture pulse-echo imaging with rectangular boundary arrays (acoustic imaging)," *IEEE Transactions on Image Processing*, vol. 2, pp. 68-79, 1993.

[12] J. A. Johnson, M. Karaman, and P. Khuri-Yakub, "Image formation and restoration using multi-element synthetic array processing," *Proceedings of SPIE The International Society for Optical Engineering*, 2002.